

Numerical modeling of an anode-supported SOFC button cell considering anodic surface diffusion

Yixiang Shi, Ningsheng Cai*, Chen Li

Key Laboratory for Thermal Science and Power Engineering of Ministry of Education, Tsinghua University, Beijing 100084, China

Received 20 July 2006; received in revised form 25 October 2006; accepted 27 October 2006

Available online 18 December 2006

Abstract

A two-dimensional isothermal mechanistic model of an anode-supported solid oxide fuel cell was developed based on button-cell geometry. The model coupled the intricate interdependency among the ionic conduction, electronic conduction, gas transport, and the electrochemical reaction processes. All forms of polarizations were included. The molecular diffusion, Knudsen diffusion, as well as the simplified competitive adsorption and surface diffusion were also considered. An electric analogue circuit was used to determine the effective hydrogen diffusivity. The model results showed good agreement with the published experimental data in different H_2 – H_2O mixtures without any other calibrations after the parameter estimation according to the experimental data in baseline operating condition. The distributions of species concentration and current density were predicted and the effects of cathode area, gas components, and anode thickness on the cell performance were studied.

© 2006 Elsevier B.V. All rights reserved.

Keywords: Solid oxide fuel cell; Anode-supported; Surface diffusion; Modeling

1. Introduction

Solid oxide fuel cells (SOFCs) are energy conversion devices, which produce electricity and heat directly from electrochemical oxidation of the fuel. A PEN (positive electrolyte negative) structure is the main component of SOFC, which usually consists of two ceramic electrodes, anode layer and cathode layer, separated by a dense electrolyte layer. The electrodes are porous to facilitate the transport of fuel and oxidant from gas channel to the three phase boundaries where electrochemical reactions occur. The electrolyte is dense to keep the gases separated to form the oxygen concentration difference between the anode and the cathode. Oxygen ions are produced at the three phase boundaries near the cathode/electrode interface, and are transported by a solid-state migration mechanism through the electrolyte to the anode/electrolyte interface, where oxygen ions react with fuel. Products molecules then transport back to the fuel channel through pores.

The relative high operating temperature of SOFC can result in highly efficient conversion to power and heat for cogen-

eration or for a bottom cycle [1]. Some demonstrations have indicated that the SOFC hybrid systems can have a higher efficiency, and have both less pollutant emissions and lower greenhouse gas emissions than other alternatives [2]. With rising fuel prices and stricter emission control regulations, these capabilities make SOFCs even more attractive. However, SOFCs also possess some serious disadvantages in fabrication, sealing and operation, etc. A number of researchers are focusing on intermediate temperature solid oxide fuel cells (IT-SOFCs) between 823 and 1073 K, allowing for a wider range of materials and more cost-effective SOFC fabrication [3,4]. Anode-supported SOFC is one of the attempts to IT-SOFCs, in which the anode is the support structure and is the thickest component in the PEN. The main advantage of the anode-supported SOFCs is the substantially lower ohmic resistance of the electrolyte, and consequently the lower operating temperature. However, it is generally accepted that the area specific resistance of IT-SOFCs may be larger than high-temperature SOFCs. This is due to activation, and perhaps concentration overpotential, which can often outweigh the ohmic contribution [5]. Thus, many efforts in SOFC technology development have been devoted to improve the electrode structure and electrolyte, aiming at obtaining a higher and more stable electrochemical performance [6,7].

* Corresponding author. Tel.: +86 10 62789955; fax: +86 10 62789955.
E-mail address: cains@tsinghua.edu.cn (N. Cai).

Nomenclature

c	concentration (mol m^{-3})
D	diffusion coefficient ($\text{m}^2 \text{s}^{-1}$)
F	Faraday constant ($96,485 \text{ C mol}^{-1}$)
ΔG	electrochemical reaction activation energy (J mol^{-1})
i	current density (A m^{-2})
i_0	exchange current density (A m^{-2})
I	total current density
L	thickness
M_i	molecular weight of species i
m, n	coefficient in i_0 calculation
n	mole fraction
N	mole flux ($\text{mol m}^{-2} \text{s}^{-1}$)
p	pressure (Pa)
Q	source term of charge balance equations (A m^{-3})
\bar{r}	average pore size (μm)
R	gas constant ($8.314 \text{ J mol}^{-1} \text{ K}^{-1}$)
R_i	source term of mass balance equations ($\text{kg m}^{-3} \text{s}^{-1}$)
S_{TPB}	TPB active area per unit volume ($\text{m}^2 \text{m}^{-3}$)
T	temperature (K)
V	voltage (V)
x_i	mole fraction of species i
w_i	mass fraction of species i

Greek letters

α	transfer coefficient
ε	porosity
η	overpotential (V)
Θ	relative coverage of hydrogen on the TPB surface
ρ	density (kg m^{-3})
σ	conductivity (S m^{-1})
τ	tortuosity

Subscripts

an	anode
avg	average
ca	cathode
elec	electronic
ion	ionic
inter	interface

Subscripts

bulk	bulk phase
eff	effective
Kn	Knudsen
MS	Maxwell–Stefan
surf	surface phase
TPB	three phase boundary

transport processes within the cell, and can be used to study the effects of operating condition and electrode design parameters on the cell performance. It is of great value for mathematic model in reducing the time and cost in SOFC development if the model can predict the detailed processes of reaction and transport incorporated with the experimental data. Many researchers have studied these complex transport and reaction processes through either experiment or numerical modeling. However, due to a lack in understanding the intricacy transport processes, and the calculation complexity, it is still difficult to build a detailed mechanistic model. Traditional models usually need to adjust many parameters to fit the experimental data, and when the operating conditions changed, the model parameters have to be adjusted again to fit the experimental data. Especially for anode-supported SOFC, the existing models in open literature usually calculate the concentration polarization by using a semi-empirical formulation [3,4]. The bulk diffusion considering the molecular and Knudsen diffusion are treated as the main sources of diffusion resistances. In this case, the tortuosities have to be tuned in the range of 10–17 to generate relatively higher anodic concentration overpotentials, then to fit to the experimental polarization curves. However, the modern anode tortuosities measured in experiments are mainly in the range of 2.5–3.5 [8]. This suggests the tuned tortuosity values are not consistent with the fact that the tortuosity is only a physical property parameter. Williford et al. [8] developed a semi-empirical model of anodic concentration polarization considering the competitive adsorption and surface diffusion. Although the model applicability should be further improved and the transport mechanisms should be further clarified through more detailed experiments, it still suggested that the diffusion resistance of modern porous ceramic anode materials is not only in the bulk of the material, but also is near the electrode/electrolyte interface. Models incorporating such concepts can predict the limiting current behavior and the performance envelopes more accurately.

In this paper, a two-dimensional isothermal mechanistic model of an anode-supported solid oxide fuel cell to describe the intricate interdependency among the ionic conduction, electronic conduction, gas transport and electrochemical processes is presented. The molecular diffusion, Knudsen diffusion, competitive adsorption near the reactive sites, and the surface diffusion are considered to escape from the unreasonable adjustment of tortuosities in various H_2 – H_2O mixtures. To improve the model generality, the general form of Butler–Volmer equation was used to solve the cell current densities and all forms of polarizations numerically. The exchange current densities were formulated as a general formulation. According to the polarization curve in a predefined base case, some parameters, which are difficult to be achieved from experiments or from published literatures were estimated.

2. Model development

2.1. Model assumptions

Consider a typical anode-supported solid oxide fuel cell, as shown in Fig. 1.

Since experimental studies on SOFC are expensive, time-consuming and labor-intensive, mathematical model is essential for SOFC study. Detailed mathematic model can help researchers to understand the complex, coupled reactions and

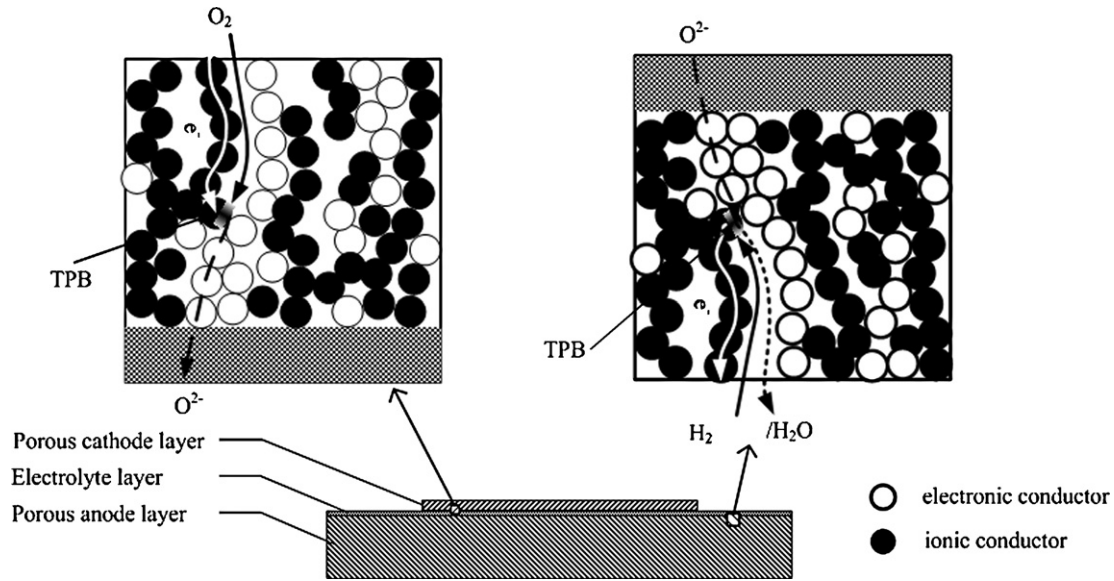


Fig. 1. Schematic diagram of anode-supported SOFC button cell.

Model assumptions are listed as follows:

- (1) Steady state conditions assumption is applied in this model;
- (2) The reactant gas mixtures are approximated as ideal gases, thus gas mixture physical properties such as specific viscosity, density, etc., can be easily estimated according to the mixed gas composition;
- (3) Since the button cell is relative small, the temperature variation across the cell is small, thus model is assumed as isothermal and the physical properties are evaluated at the average cell temperature;
- (4) The reaction active sites are uniformly distributed in the electrode. The two conducting phases, electronic conducting phase and ionic conducting phase, are considered to be continuous and homogeneous. Since the material properties of both electronic conductor and ionic conductor are only represented by model parameters, the model itself could be assumed to be not material-specific;
- (5) The pressure gradient in the porous flow is neglected.

Furthermore, the boundary conditions of concentration and potential is assumed uniform at the electrode/gas channel interface.

2.2. Model geometry

The model geometry is based on a button cell. Due to the cell symmetry conditions, the two-dimensional axial symmetry coordinate is adopted as that illustrated in Fig. 2.

2.3. Charge balance

2.3.1. General formulation of charge balance governing equation

The charge balance control domains include the anode, the cathode and the electrolyte. At the electrodes, electrons and oxygen ions are served as conductive particles, and at the electrolyte, the conductive particles are only oxygen ions. The charge balance can be formulated by the point form of Ohm's law in a stationary coordinate system:

$$-\nabla \cdot (\sigma \nabla V) = Q_j \tag{1}$$

The current source term Q_j can be calculated by the equation below.

$$Q_j = \pm i_{\text{trans}} S_{\text{TPB}} \tag{2}$$

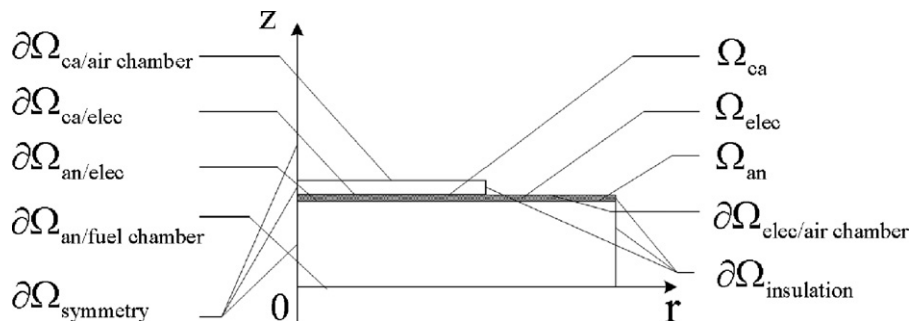


Fig. 2. Schematic diagram of model geometry.

The choice of the sign before the term on the right side of equation depends on the conductor phase type and calculation domain. For ionic charge balance at the anode, the current source term should be positive as the anode is served as the ion sources and the ions carries negative electric charge, while, for electronic charge balance at the anode, the current source term should be negative to keep the charge balance. Similar to the anode, the cathode is served as ion sinks and electron sources, thus, the current source term is negative when considering the ionic charge balance and is positive when considering electronic charge balance.

S_{TPB} in above equation is the electrochemical reaction active area per unit volume, this parameter has been formulated by some researchers by using the particle coordination number, together with percolation theory as follows [9–11]. However, to simplify the calculation, this parameter was kept as a constant in this paper.

The i_{trans} is the local charge transfer current density and can be calculated by generalized Butler–Volmer equation:

$$i_{\text{trans}} = i_0 \left(\frac{c_{\text{react}}}{c_{\text{react}}^I} \exp\left(\alpha \frac{n_e F \eta}{RT}\right) - \frac{c_{\text{prod}}}{c_{\text{prod}}^I} \exp\left(-(1-\alpha) \frac{n_e F \eta}{RT}\right) \right) \quad (3)$$

where i_0 is the exchange current density; α the charge transfer coefficient; F the Faraday constant; R the gas constant; c_{react} , c_{react}^I , c_{prod} , c_{prod}^I are the reactant and product concentrations at the reaction active sites and the electrode/channel interface; η the local overpotential, defined as follows [11]:

$$\eta = V_{\text{elec}} - V_{\text{ion}} - V_{\text{ref}} \quad (4)$$

where V_{ref} is the relative potential difference between the electronic and ionic conductors at the reference state. In this paper, the open-circuit state was chosen as the reference state.

2.3.2. Charge balance at the cathode layer

The cathode usually gives large contribution to potential loss. For conventional cathode material, electrochemical reaction transfers the current from ionic conductor to electronic conductor. The voltage loss mainly consists of Ohmic overpotential in the electronic and ionic conductors, activation overpotential for electron transfer reaction, and concentration overpotential, due to mass transport resistance. To deal with the concentration overpotential, the gas species concentration differences between the reactive sites and electrode/air channel interface are considered.

$$\frac{c_{\text{react,ca}}}{c_{\text{react,ca}}^I} = \frac{c_{\text{O}_2,\text{ca}}^{\text{TPB}}}{c_{\text{O}_2,\text{ca}}^{\text{bulk}}}, \quad c_{\text{prod,ca}}^{\text{TPB}} = c_{\text{prod,ca}}^{\text{bulk}} \quad (5)$$

where $c_{\text{O}_2,\text{ca}}^{\text{TPB}}$ and $c_{\text{O}_2,\text{ca}}^{\text{bulk}}$ are the oxygen concentrations at the reaction active site and at the electrode/gas chamber interface.

The exchange current density is defined as the current density of the charge-transfer reaction at the dynamic equilibrium potential. Under this circumstance, the forward and reverse current

densities are equal to i_0 . Thus i_0 is a measure of the electrocatalytic activity at the electrode/electrolyte interface or the TPB for a given electrochemical reaction [12]. The cathodic exchange current density can be formulated as [13]:

$$i_{0,\text{ca}} = i_{0,\text{ca}}^I \frac{(p_{\text{O}_2,\text{ca}}/p_{\text{O}_2,\text{ca}}^*)^{1/4}}{1 + (p_{\text{O}_2,\text{ca}}/p_{\text{O}_2,\text{ca}}^*)^{1/2}} \quad (6)$$

where $i_{0,\text{ca}}^I$ is used as an empirical parameter to fit experimental observation; p_{O_2} the local oxygen partial pressure; $p_{\text{O}_2,\text{ca}}^*$ is formulated as the Arrhenius form as below:

$$p_{\text{O}_2,\text{ca}}^* = A_{\text{O}_2} \exp\left(\frac{-E_{\text{O}_2}}{RT}\right) \quad (7)$$

where $A_{\text{O}_2} = 4.9E8$ bar, and $E_{\text{O}_2} = 200$ kJ mol⁻¹.

By setting $V_{\text{ref,an}}$ to zero, the cathode reference potential $V_{\text{ref,ca}}$ will be the open circuit voltage:

$$V_{\text{ref,ca}} = E^0 - \frac{RT}{2F} \ln\left(\frac{p_{\text{O}_2,\text{ca}}^{0.5} p_{\text{H}_2,\text{a}}}{p_{\text{H}_2\text{O},\text{a}}}\right) \quad (8)$$

where E^0 is the ideal Nernst potential and can be calculated as:

$$E^0 = -\frac{\Delta G^\circ}{n_e F} \quad (9)$$

where ΔG° is the change of standard-state Gibbs free energy between the products and the reactants.

However, calculated open circuit voltages usually are a little higher than the experimental values. In this paper, this difference was treated as the so called “leak overpotential” denoted by η_{leak} .

Then, the ionic charge balance at the cathode can be written as:

$$\begin{aligned} & -\nabla \cdot (\sigma_{\text{ion,ca}} \nabla V_{\text{ion,ca}}) \\ & = -i_{0,\text{ca}} S_{\text{TPB,ca}} \left(\frac{c_{\text{O}_2}^{\text{TPB}}}{c_{\text{O}_2}^{\text{bulk}}} \exp\left(\frac{\alpha n_e F (V_{\text{elec,ca}} - V_{\text{ion,ca}} - V_{\text{ref,ca}})}{RT}\right) \right) \\ & \quad \times \exp\left(-\frac{(1-\alpha)n_e F (V_{\text{elec,ca}} - V_{\text{ion,ca}} - V_{\text{ref,ca}})}{RT}\right) \end{aligned} \quad (10)$$

Similar to the ionic charge balance, the electronic charge balance at the cathode can be written as:

$$\begin{aligned} & -\nabla \cdot (\sigma_{\text{elec,ca}} \nabla V_{\text{elec,ca}}) \\ & = i_{0,\text{ca}} S_{\text{TPB,ca}} \left(\frac{c_{\text{O}_2}^{\text{TPB}}}{c_{\text{O}_2}^{\text{bulk}}} \exp\left(\frac{\alpha n_e F (V_{\text{elec,ca}} - V_{\text{ion,ca}} - V_{\text{ref,ca}})}{RT}\right) \right) \\ & \quad \times -\exp\left(-\frac{(1-\alpha)n_e F (V_{\text{elec,ca}} - V_{\text{ion,ca}} - V_{\text{ref,ca}})}{RT}\right) \end{aligned} \quad (11)$$

2.3.3. Charge balance at the anode layer

Similar to cathode, for conventional anode material, Ni/YSZ mixture, electrochemical reaction transfers the current from ionic conductor YSZ to electronic conductor Ni.

According to the general governing equation of charge balance, the ionic current balance at the anode is given as:

$$\begin{aligned} & -\nabla \cdot (\sigma_{\text{ion,an}} \nabla V_{\text{ion,an}}) \\ & = -i_{0,\text{an}} S_{\text{TPB,an}} \left(\frac{c_{\text{H}_2}^{\text{TPB}}}{c_{\text{H}_2}^{\text{bulk}}} \exp \left(\frac{\alpha n_e F (V_{\text{elec,an}} - V_{\text{ion,an}} - V_{\text{ref,an}})}{RT} \right) \right) \\ & \quad - \frac{c_{\text{H}_2\text{O}}^{\text{TPB}}}{c_{\text{H}_2\text{O}}^{\text{bulk}}} \exp \left(- \frac{(1 - \alpha) n_e F (V_{\text{elec,an}} - V_{\text{ion,an}} - V_{\text{ref,an}})}{RT} \right) \end{aligned} \quad (12)$$

The calculation of hydrogen species at the TPB active sites will be discussed in Section 2.4.

The exchange current density of hydrogen electrochemical oxidation was proposed in this paper.

$$i_{0,\text{an}} = i_{0,\text{an}}^I \left(\frac{c_{\text{H}_2}}{c_{\text{base,H}_2}} \right) \exp \left(\frac{-120000}{RT} \right) (p_{\text{O}_2,\text{an}})^{0.133} \quad (13)$$

where $i_{0,\text{an}}^I$ is an adjustable parameter to fitting the experimental data in base case. $c_{\text{base,H}_2}$ the hydrogen concentration in the base case.

The $p_{\text{O}_2,\text{an}}$ is the water vapor partial pressure at the anode due to hydrogen oxidation equilibrium and could be calculated as:

$$p_{\text{O}_2,\text{an}} = \left(\frac{p_{\text{H}_2\text{O}}}{K_{\text{eq,H}_2} p_{\text{H}_2}} \right)^2 \quad (14)$$

where $K_{\text{eq,H}_2}$ is the equilibrium constant of hydrogen oxidation reaction.

Similar to the ionic charge balance, the electronic charge balance at the anode can be written as:

$$-\nabla \cdot (\sigma_{\text{elec,an}} \nabla V_{\text{elec,an}}) = -i_{\text{trans,an}} S_{\text{TPB,an}} \quad (15)$$

2.3.4. Charge balance at the electrolyte layer

For the electrolyte layer, there is only ion conductor. And there are no current sources or sinks. Consequently, only Ohmic polarization exists in the electrolyte and the charge balance governing equation can be written as:

$$-\nabla \cdot (\sigma_{\text{ion,electrolyte}}^{\text{eff}} \nabla V_{\text{ion,electrolyte}}) = 0 \quad (16)$$

where $\sigma_{\text{ion,electrolyte}}^{\text{eff}}$ is the effective conductivity of the YSZ electrolyte.

2.4. Mass balance

2.4.1. General formulation of mass balance governing equation

Diffusion inside the porous media is important for fuel cell reactions. Within a pore, three fundamentally different types of diffusion mechanisms are distinguished [14].

- (1) Free molecular diffusion is significant for large pore size and high pressures. In this case, molecule-molecule collisions dominate over molecule-wall collisions.
- (2) Knudsen diffusion becomes predominant when the mean-free path of the molecular species is much larger than the

pore diameter and hence molecule-wall collisions become important.

- (3) Surface diffusion of adsorbed molecular species along the pore wall surface becomes dominant for micro pores and for strongly adsorbed species. At high currents and high fuel utilization, the competitive adsorption and surface diffusion of hydrogen may be responsible to the high interface diffusion resistance [8].

The steady state mass balance can be formulated:

$$\nabla \cdot j_i = R_i \quad (17)$$

where R is the source term of mass balance, and can be formulated as the reaction rate of the electrochemical and chemical reactions; j the molecular mass flux and can be formulated as a function of a diffusion driving force. For species i , according to the generalized formulation of Fick's law, the governing equations of mass balance could be expressed as:

$$-\nabla \cdot \left(\rho w_i \sum_{k=1}^N D_{ik}^{\text{eff}} d_k \right) = R_i \quad (18)$$

where w_i is the mass fraction of species i ; d_k the generalized driving force. Considering the driving forces through concentration and pressure, the d_k can be formulated as:

$$d_k = \nabla x_k \quad (19)$$

D_{ik}^{eff} is the effective multi-component diffusivity between components i and k . In order to solve Eq. (18), the multi-component diffusivity must be specified.

Free molecular and Knudsen diffusion mechanisms occur together and it is prudent to take both of them into account rather than assume that one or the other mechanism is controlling. It is generally agreed that the dusty gas model is the most convenient approach to describe the combined bulk and Knudsen diffusion [15]. The principle of the dusty gas model is based on the Maxwell–Stefan diffusion by considering the pore wall as consisting of giant molecules uniformly distributed in space. In order to account for the tortuous path of the molecule rather than along the radial direction and the porosity of the electrode for the fact that diffusion occurs only in the pore space, an effective Maxwell–Stefan diffusion coefficient and Knudsen diffusion coefficient can be formulated as:

$$D_{ik}^{\text{MS,eff}} = \frac{\varepsilon}{\tau} D_{ik}^{\text{MS}} \quad (20)$$

$$D_i^{\text{Kn,eff}} = \frac{\varepsilon}{\tau} D_i^{\text{Kn}} \quad (21)$$

where, ε denotes the electrode porosity and τ denotes the electrode tortuosity.

Then, the bulk effective multi-component diffusivities can be calculated by:

$$D_{ik}^{\text{bulk,eff}} = \frac{1}{1/D_{ik}^{\text{MS,eff}} + 1/D_i^{\text{Kn,eff}}} \quad (22)$$

For species O_2 , N_2 and H_2O , the effective diffusivities are just the bulk effective multi-component diffusivities. For hydrogen

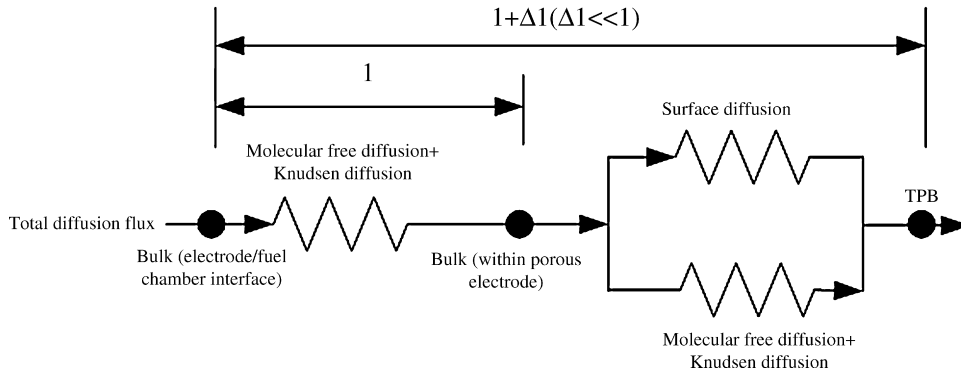


Fig. 3. Electric analogue circuit of H₂ diffusion.

species, to achieve the H₂ concentration at the TPB, $c_{\text{H}_2}^{\text{TPB}}$, the competitive adsorption and surface diffusion mechanisms were taken into account.

The electric analogue circuit of hydrogen diffusion is assumed as shown in Fig. 3.

As the figure shows, the diffusion flux from fuel channel/electrode interface to a certain place within the porous electrode is equal to the diffusion flux from this certain place to the three phase boundary. Here, l is the distance from anode/electrolyte interface to a certain position within the electrode and Δl the distance from a certain position within the electrode to the three phase boundaries. Δl is much shorter than l , and the effective diffusivity $D_{\text{H}_2}^{\text{eff}}$ can be formulated as following Eq. [8]:

$$D_{\text{H}_2}^{\text{eff}} = (D_{\text{H}_2}^{\text{bulk,eff}})^{\Theta} (D_{\text{H}_2}^{\text{surf}})^{1-\Theta} \quad (23)$$

where Θ is the relative coverage of hydrogen on the TPB surface, $D_{\text{H}_2}^{\text{surf}}$ the surface diffusion coefficient and can be formulated as [8]:

$$D_{\text{H}_2}^{\text{surf}} = \frac{(D_{\text{H}_2,0}^{\text{surf}})^{1-\Theta} (D_{\text{H}_2,1}^{\text{surf}})^{\Theta}}{1-\Theta} \quad (24)$$

where $D_{\text{H}_2,0}^{\text{surf}}$ is the surface diffusion coefficient of hydrogen as zero coverage is approached, and $D_{\text{H}_2,1}^{\text{surf}}$ is that as full coverage is approached at very low relative coverage and high temperatures, $D_{\text{H}_2,0}^{\text{surf}}$ may approach the bulk gas value due to the high availability of vacant surface sites for diffusion by atomic hopping mechanisms. Thus, to simplify the calculation, it is reasonable to assume the $D_{\text{H}_2,0}^{\text{surf}}$ is equal to $D_{\text{H}_2}^{\text{bulk,eff}}$. Also, we assumed that the relative coverage of hydrogen is approximately equal to mole fraction of hydrogen in this paper. The ratio of $D_{\text{H}_2}^{\text{bulk,eff}}$ and $D_{\text{H}_2,1}^{\text{surf}}$ remains to be an adjustable parameter in the model.

2.4.2. Mass balance at the cathode

According to the Faraday's law, the relationship between the mass balance source term and the current source term at the cathode can be built:

$$R_{\text{O}_2} = \frac{i_{\text{trans,O}_2} S_{\text{TPB}} M_{\text{O}_2}}{4F} \quad (25)$$

The reaction rate of nitrogen at the cathode is zero and the mass fraction of nitrogen can be calculated by:

$$w_{\text{N}_2} = 1 - w_{\text{O}_2} \quad (26)$$

2.4.3. Mass balance at the anode

At the anode, the reactions include the electrochemical reactions of hydrogen and carbon monoxide and the shifting reactions.

Similar to the cathode, the relationship between the mass balance source term and the current source term for the electrochemical reactions at the anode can be built:

$$R_{\text{H}_2} = \frac{i_{\text{trans,an}} S_{\text{TPB}} M_{\text{H}_2}}{2F} \quad (27)$$

$$R_{\text{H}_2\text{O}} = \frac{-i_{\text{trans,an}} S_{\text{TPB}} M_{\text{H}_2\text{O}}}{2F} \quad (28)$$

From the mass balance at the anode, the species concentration at the electrode, c_i , can be solved.

2.5. Boundary conditions

In order to solve the coupled partial differential equation systems of charge and mass balance, the boundary conditions of all outer interfaces are specified as in Table 1.

In Table 1 the difference between $V_{\text{cell,ca}}$ and $V_{\text{cell,an}}$ should be the cell voltage used in the calculation. Here, we choose $V_{\text{cell,an}} = 0$ V. $w_{i,\text{bulk}}$ in the table is the mass fraction of species i in the fuel/air channel. The boundary condition "insulation" denotes no flux through the boundary. the boundary condition "symmetry" denotes that the partial derivate of the parameter at the boundary is zero.

2.6. Solution algorithm

By given a specified value of cell voltage, the parameters (e.g. current density, species concentration) distributions can be achieved. The calculation was done by using the finite element commercial software COMSOL MULTIPHYSICS®.

Table 1
Boundary conditions

	Ionic charge balance	Electronic charge balance	Mass balance
$\partial\Omega_{ca}/\text{air chamber}$	Insulation	$V_{\text{cell,ca}}$	$w_{\text{O}_2,\text{bulk}}, w_{\text{N}_2,\text{bulk}}$
$\partial\Omega_{\text{elec}}/\text{air chamber}$	Insulation	Insulation	Insulation
$\partial\Omega_{ca}/\text{elec}$	Continuity	Insulation	Insulation
$\partial\Omega_{an}/\text{elec}$	Continuity	Insulation	Insulation
$\partial\Omega_{an}/\text{fuel chamber}$	Insulation	$V_{\text{cell,an}}$	$w_{\text{H}_2,\text{bulk}}, w_{\text{H}_2\text{O},\text{bulk}}$
$\partial\Omega_{\text{symmetry}}$	Symmetry	Symmetry	Symmetry
$\partial\Omega_{\text{others}}$	Insulation	Insulation	Insulation

Table 2
PEN geometries and properties parameters

Layer	Cathode	Electrolyte	Anode
Radius, R (cm)	0.8	1.3	1.3
Thickness, d (μm)	60	10	1100
Porosity, ε	0.35	–	0.35
Tortuosity, τ	3.5	–	3.5
Average pore radius, r_p (μm)	0.5	–	0.5
Ionic conductor conductivity, σ_{ion} (S m^{-1})	$3.34 \times 10^4 \exp(-10,300/T)$	$3.34 \times 10^4 \exp(-10,300/T)$	$3.34 \times 10^4 \exp(-10,300/T)$
Electronic conductor conductivity, σ_{elec} (S m^{-1})	$\frac{42 \times 10^6}{T} \exp\left(\frac{-1150}{T}\right)$	–	2×10^6

According to the current density distribution, the average current density can be calculated by:

$$I_{\text{avg}} = \frac{I_{\text{total}}}{S} = \frac{1}{R_{\text{inter}}^2} \int_0^R 2ri_{\text{local}} dr \quad (29)$$

where R_{inter} is the radius of the interface we concerned; i_{local} the local current density.

In order to generate the full polarization curve, the calculation should be done over a range of cell voltages to calculate the corresponding average current density.

3. Results and discussions

3.1. Parameter settings and model validations

Some of the model input parameters are listed in Table 2.

The operation conditions in the base case are listed in Table 3. Since some of the parameters could not be achieved directly from experiments or published literature, the tuning processes have to be involved in the study. One of the adjustable parameter, leak overpotential, could be estimated as the difference between the experimental and calculated open circuit voltage using Eq. (9). This parameter was kept as a constant 0.05 for all of the calculations. The adjustable parameters $i_{0,\text{an}}^I$, $i_{0,\text{ca}}^I$ and S_{TPB} were varied in order to bring the model results into closer agreement with

Table 3
Operating conditions in the base case

Parameters	Value
Pressure, p (Pa)	101,325
Temperature, T ($^{\circ}\text{C}$)	800
Fuel composition	85% H_2 and 15% H_2O
Oxidant composition	21% O_2 and 79% N_2 .

the experimental data in the base case. It should be noted that the adjustable parameter $D_{\text{H}_2}^{\text{bulk,eff}}/D_{\text{H}_2,1}^{\text{surf}}$, was varied in order to assure the agreement of the modeling results and experimental data in the case when the fuel composition is 20% H_2 and 80% H_2O . Then the model could be validated further in some other cases without changing these parameters. The values of adjustable parameters are summarized in Table 4.

Then, by changing the fuel composition and cell voltage, the cell performances obtained from the model for various compositions are compared with the experimental data at 800 $^{\circ}\text{C}$ with air as the oxidant as shown in Fig. 4:

The results showed that the calculated polarization curves agreed very well with the experimental data in most cases except that in the case of pure hydrogen and the case of 50% H_2 , 50% H_2O . For the 50% H_2 –50% H_2O fuel mixtures, the model results overestimate the cell performance when the current density is relatively high. And for the pure hydrogen, the model results slightly underestimate cell performance in the overall extent of current density. In fact, the simplification to the competitive adsorption and surface diffusion procedure might be the important source of the derivation. Owing to the consideration of detailed processes of adsorption and surface diffusion, the model can be used to predict the cell performances in a large extent of current density while also in a large fuel composition

Table 4
Adjustable model parameters

Parameter	Value
Leak overpotential, η_{leak} (V)	0.05
Adjustable parameter, $i_{0,\text{an}}^I$ (A m^{-2})	1.079E4
Adjustable parameter, $i_{0,\text{ca}}^I$ (A m^{-2})	2E3
TPB area per unit volume, S_{TPB} ($\text{m}^2 \text{m}^{-3}$)	3.225E5
Adjustable parameter, $D_{\text{H}_2}^{\text{bulk,eff}}/D_{\text{H}_2,1}^{\text{surf}}$	8

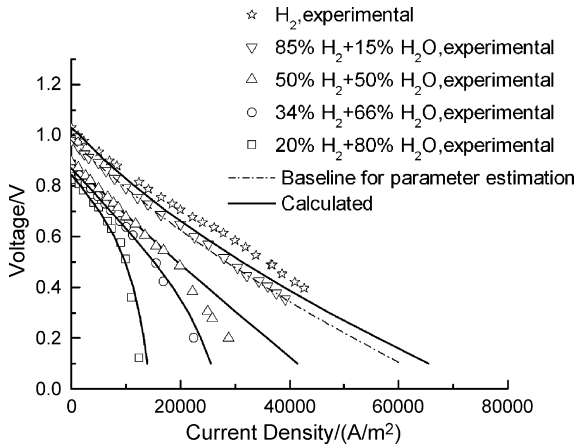


Fig. 4. Results of parameter estimation and model validation.

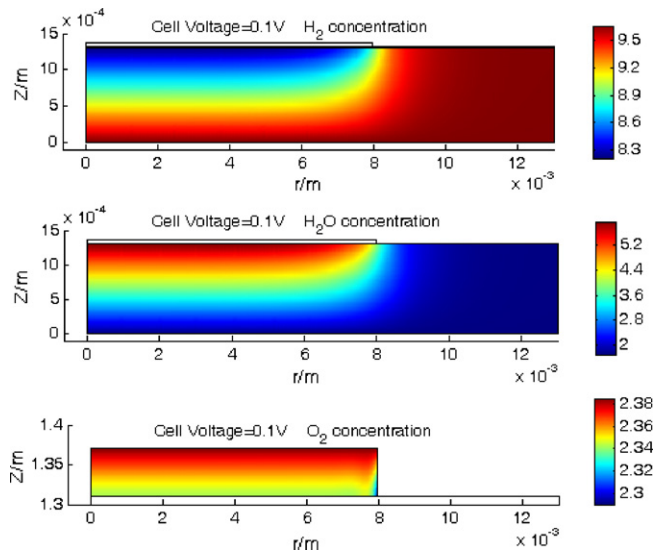


Fig. 6. Surface plots of H₂, H₂O, O₂ concentration.

extent without any other calibrations after the parameter estimation according to the experimental *I–V* curve in the base case. The results suggested that with the amount of H₂ increasing in the fuel, the open circuit voltage as well as the maximum current density decreased. When H₂ concentration is low, substantial concentration polarization was present as evidenced by the observation of a limiting current density.

For making detailed comparison, Fig. 5 shows the modeling results without the modifications to the hydrogen concentration at the three phase boundaries while using the same parametric set with baseline condition except that the tortuosity is treated as an adjustable parameter to assure the agreement of the modeling results and experimental data. We can see that when the fuel composition is 85% H₂ and 15% H₂O, the value of tortuosity is 3.5 and this value agreed well with the published experimental data. However, when the fuel composition is 20% H₂ and 80% H₂O, the model could not predict the experimental data well until the tortuosity in the model was adjusted to 14.

3.2. Species concentration distribution in the base case

The distributions of the H₂, H₂O concentrations at the anode and the O₂ concentration at the cathode in the base case are shown in Fig. 6.

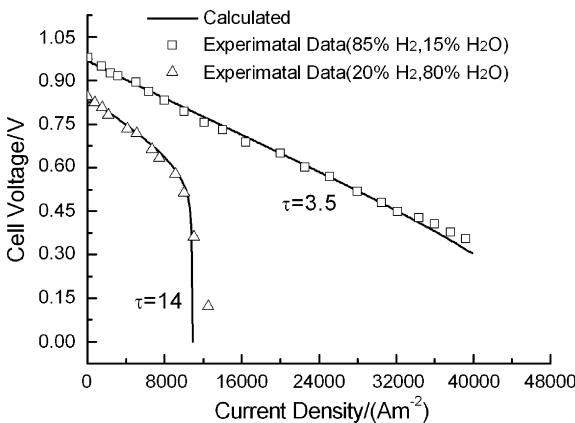


Fig. 5. Modeling results by tuning tortuosity.

The H₂ concentration reduces fast along the *z* direction in the region opposite to the cathode and reduces more gradually in the region outside of cathode radius, and this un-uniformity is due to the asymmetric electrode of the button-cell. Contradict to H₂ distribution, the H₂O concentration rises along *Z* direction. The O₂ concentration distribution remains relatively uniform throughout the cathode. This suggests that the O₂ is sufficient even just using air as oxidant for electrochemical reaction and that the cathodic concentration overpotential can be neglected compared to relatively large anodic concentration overpotential.

3.3. Current densities distribution

Fig. 7 gives the electronic current density and ionic current density distributions at the anode, cathode and electrolyte along the cell thickness direction (*r*=0). As shown in the figure, most of the electrons are generated near the electrode/electrolyte interface where ions are eliminated. The calculations suggest that the electrochemical reactions mainly occur at the electrode/electrolyte interface. It should be noted that with decreasing of H₂ content in the fuel, the reaction occurs at a position further from the anode/electrolyte interface. In fact,

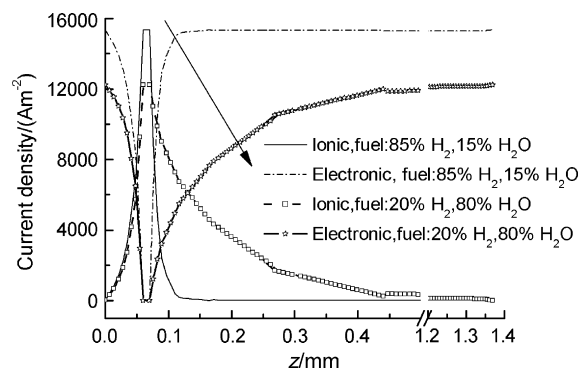


Fig. 7. Distributions of electronic and ionic current density along the button-cell thickness direction (*r*=0).

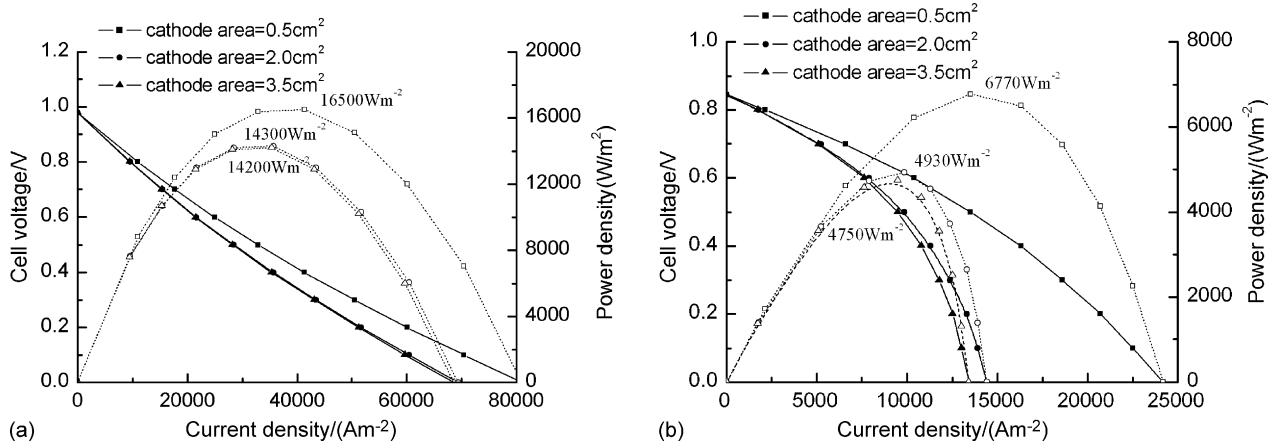


Fig. 8. Effects of cathode area on the cell performance for (a) fuel composition: 85% H₂ and 15% H₂O; (b) fuel composition: 20% H₂ and 80% H₂O. (anode area: 5.31 cm²).

the reactions always occur at the sites where the total resistances, including mass transport resistance, electrochemical activation resistance and also the charge transfer resistance, reach the minimum [16,17]. Lower H₂ concentration will lead to larger diffusion resistance, so at this time, it is much more difficult for the reactant gas to approach the anode/electrolyte interface.

3.4. Effects of cathode area on cell performance

Fig. 8 shows cell polarization curves as well as power density versus current density traces, for cells with cathode areas of 0.5, 2, 3.5 cm² at 800 °C. Both the current density and power density are determined on the basis of the cathode area.

As shown in Fig. 8(a), the fuel composition is 85% H₂ and 15% H₂O. There was no obvious limiting current density even at the highest current density. The maximum power density is approximately 16,500 W m⁻² with the 0.5 cm² cathode, while that for the cell with the 2 cm² cathode is ~14,300 W cm⁻². The results show that the difference is 2200 W m⁻², with the relative difference is ~13.3%. When the cathode area increase from 2 to 3.5 cm², the difference of maximum power density is

about only 100 W cm⁻². This difference can almost be neglected even the cathode area is doubled. Similar to this case, as shown in Fig. 8(b), the fuel composition is 20% H₂, 80% H₂O. The maximum power density is 6770 W m⁻² with 0.5 cm², while that for the cell with the 2 cm² cathode is about ~4930 W m⁻². The difference is about 1840 W cm⁻², and the relative difference is almost ~27.2%. When the cathode area increase from 2 to 3.5 cm², the difference is about 180 W m⁻², and the relative difference is about ~3.6%. Thus, a preliminary conclusion is that the cell performance will be better with decreasing cathode area while keeping anode area as a fixed valued. The effect degree of cathode area will be higher with the smaller cathode or with the lower H₂ content fuel mixtures. This conclusion is qualitatively constant with the analysis in the published literature [4]. The source of potential differences in the reported power densities due to asymmetric electrodes lies principally in the differences in the anodic concentration polarizations. It suggests that the relatively larger anode/fuel gas interface with smaller active anode/electrolyte interface could lead to the lower gas transport resistance. In order to predict the anodic concentration polarization correctly, the cathode area should not be too small in the real experiment.

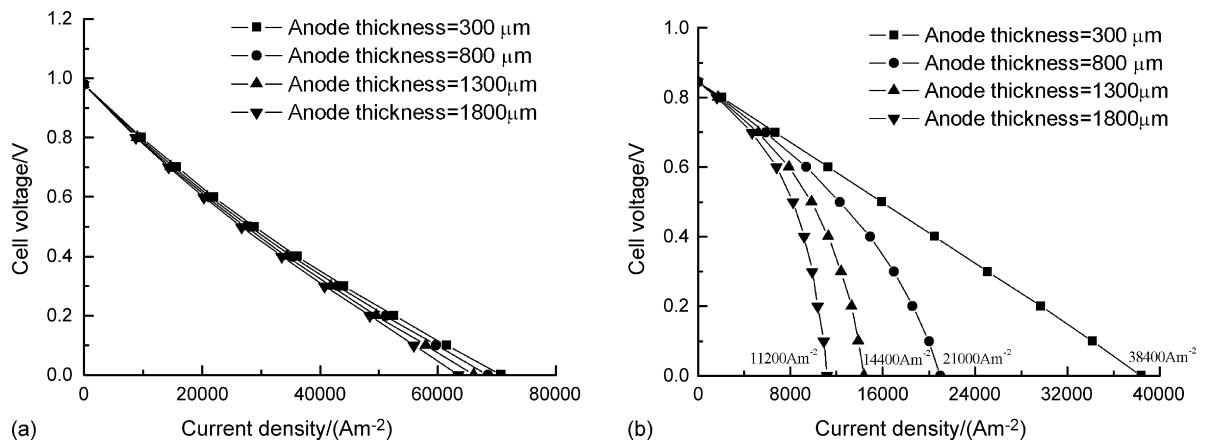


Fig. 9. Effects of anode thickness on the cell performance for (a) fuel composition: 85% H₂ and 15% H₂O; (b) fuel composition: 20% H₂ and 80% H₂O.

3.5. Effects of anode thickness with different fuel composition

Fig. 9 presents the effects of anode thickness on the cell performance. As shown in Fig. 9(a), when the fuel composition is 85% H₂ and 15% H₂O mixtures, the cell performance is slightly affected by the anode thickness and there was no obvious limiting current density even when the relatively thick anode (1800 μm) was adopted. Since the effects of anode thickness are mainly on the anodic concentration overpotential, it suggests that the anodic concentration overpotential is not obvious in this case. However, if the reactant gas concentration in the fuel is low, as Fig. 9(b) shows, the cell limiting current density decrease fast from 38,400 to 11,200 A m⁻² when the anode thickness increase from 300 to 1800 μm. Thus, in actual operation of SOFC, when the reactant concentration is low or fuel utilization is high, especially in the fuel channel downstream area, gas diffusion through a thick and porous anode will be one of the performance-limiting factors. In this case, a thinner anode layer should be adopted to reduce the large anodic concentration overpotential.

4. Conclusions

A two-dimensional isothermal mathematical model of an anode-supported solid oxide fuel cell was developed based on a button-cell geometry. The model coupled the intricate interdependency among the ionic conduction, electronic conduction, gas transport, and electrochemical processes. The model has been applied to generate polarization curves and parameter distributions for different cell configurations and specified operating conditions. All forms of the polarizations were considered, including activation polarization, Ohmic polarization, concentration polarization, and leak overpotential. For the modifications to the mass transport calculation, the molecular diffusion, Knudsen diffusion, as well as the simplified competitive adsorption and surface diffusion processes were taken into account. The validation results showed that the model agrees well with the published experimental data in different H₂–H₂O fuel mixtures without any other calibrations after the parameter estimation according to the experimental data in base-line operating condition.

The distributions of H₂, H₂O and O₂ at the electrode suggest that the O₂ is sufficient even by using air as oxidant. The cathodic concentration overpotential can be neglected compared to relatively large concentration difference at the anode if we want to simplify the calculation. The results of electronic/ionic

current densities distributions suggest that the electrochemical reactions mainly occur near the electrode/electrolyte interface and with decreasing H₂ content in the fuel, the reaction occurs at a position further from the anode/electrolyte interface. The cell performance will be better with a smaller cathode while keeping the anode area as a fixed value. The cathode area effect will be higher with the smaller cathode or with the lower H₂ content fuel mixtures. The effects of anode thickness is not obvious when the H₂ content in the fuel mixtures is relatively high, while that is very significant if the H₂ content in the fuel mixtures is low. This situation usually occurred at the downstream of fuel channel especially when the fuel utilization is high.

Finally, it should be noted that it is necessary to improve the competitive adsorption and surface diffusion mechanism to predict the detailed mass transport processes within the porous anode. In addition, in future work, the model will be extended to study the cell performance with multi-component fuel, which may be more practical in actual SOFC applications.

References

- [1] J.H. Hirschenhofer, D.B. Stauffer, R.R. Engleman, et al., Fuel Cell Handbook, 7th ed., EG&G Technical Services, Inc., West Virginia, 2004.
- [2] A.C. Casanova, S.E. Veyo. Pre-Commercial Demonstration Projects for SOFC Simple-Cycle and SOFC/Turbine Hybrid Systems [EB/OL]. <http://www.pg.siemens.de/> (2001).
- [3] Y. Jiang, A.V. Virkar, J. Electrochem. Soc. 150 (7) (2003) A942–A951.
- [4] A.V. Virkar, Low-temperature, anode-supported high power density solid oxide fuel cells with nanostructured electrodes. USA: University of Utah, Contract No: AC26-99FT40713, 2003.
- [5] P. Aguiara, C.S. Adjimana, N.P. Brandona, J. Power Sources 138 (2004) 120–136.
- [6] K. Yamaji, H. Kishimoto, Y. Xiong, et al., Solid State Ionics 175 (2004) 165–169.
- [7] R.N. Basu, G. Blass, H.P. Buchkremer, et al., J. Eur. Ceram. Soc. 25 (2005) 463–471.
- [8] R.E. Williford, L.A. Chick, G.D. Maupin, et al., J. Electrochem. Soc. 150 (8) (2003) A1067–A1072.
- [9] A.V. Virkar, J. Chen, C.W. Tanner, et al., Solid State Ionics 131 (2000) 189–198.
- [10] J. Fleig, Annu. Rev. Mater. 3 (2003) 361–382.
- [11] P. Costamagana, P. Costa, V. Antonucci, Electrochim. Acta 43 (3–4) (1998) 375–394.
- [12] H. Zhu, J. Kee Robert, J. Power Sources 117 (2003) 61–74.
- [13] H. Zhu, J. Kee Robert, M. Vinod, Janardhanan, et al., J. Electrochem. Soc. 152 (12) (2005) A2427–A2440.
- [14] R. Krishna, J.A. Wesselingh, Chem. Eng. Sci. 52 (6) (1997) 861–911.
- [15] R. Suwanwarangkul, E. Croiset, M.W. Fowler, et al., J. Power Sources 122 (2003) 9–18.
- [16] S.H. Chan, Z.T. Xia, J. Electrochem. Soc. 148 (4) (2001) A388.
- [17] S.H. Chan, X.J. Chen, K.A. Khor, J. Electrochem. Soc. 151 (1) (2004) A164.